Bioengineered Bacterial Outer Membrane Vesicles as Cell-Specific Drug-Delivery Vehicles for Cancer Therapy

Vipul Gujrati,[†] Sunghyun Kim,[†] Sang-Hyun Kim,[‡] Jung Joon Min,[§] Hyon E Choy,[§] Sun Chang Kim,[†] and Sangyong Jon[†,*]

[†]KAIST Institute for the BioCentury, Department of Biological Sciences, Korea Advanced Institute of Science and Technology (KAIST), 291 Daehak-ro, Yuseong-gu, Daejeon 305-701, Republic of Korea, [‡]The National Primate Research Center, Korea Research Institute of Bioscience and Biotechnology, Yeongudanji-ro 30, Ochang, Chungbuk 363-883, Republic of Korea, and [§]Department of Nuclear Medicine, Chonnam National University Hwasun Hospital, 322 Seoyang-ro, Hwasun, Jeonnam 519-763, Republic of Korea. S.J. conceived the project; V.G. performed the experiments; S.K. and S.H.K. supported some experiments; V.G., J.J.M., H.E.C., S.C.K., and S.J. analyzed the results; V.G. and S.J. wrote the manuscript.

ABSTRACT Advances in genetic engineering tools have contributed to the development of strategies for utilizing biologically derived vesicles as nanomedicines for achieving cell-specific drug delivery. Here, we describe bioengineered bacterial outer membrane vesicles (OMVs) with low immunogenicity that can target and kill cancer cells in a cell-specific manner by delivering small interfering RNA (siRNA) targeting kinesin spindle protein (KSP). A mutant *Escherichia coli* strain that exhibits reduced endotoxicity toward human cells was engineered to generate OMVs displaying a human epidermal growth factor receptor 2 (HER2)-specific affibody in the membrane as a targeting ligand. Systemic injection of siRNA-packaged OMVs caused targeted gene silencing and induced highly significant tumor growth regression in an animal model. Importantly, the modified OMVs were well tolerated and showed no evidence of nonspecific side effects. We propose that bioengineered OMVs have great potential as cell-specific drug-delivery vehicles for treating various cancers.

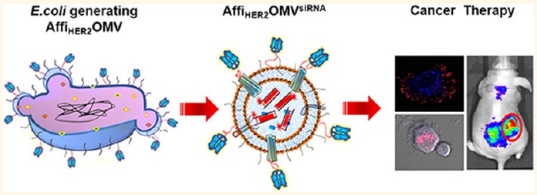

KEYWORDS: affibody · cancer therapy · drug delivery · outer membrane vesicles · siRNA

Synthetic nanomaterials, including liposomes, polymers, and metal-based nanoparticles, have been intensively studied as drug-delivery carriers for the treatment of cancers.[1−5] A few such cancer nanomedicines are undergoing clinical trials or already on the market.[6−8] In addition to synthetic nanoparticles, biological nanocarriers derived from diverse natural sources such as pathogens and mammalian cells have attracted substantial attention in recent years.[9] Such biological nanoparticles are well suited for drug-delivery purposes.[9,10] Among recently developed biological nanocarriers applicable for tumor homing and cancer therapy are macromolecular nanocages derived from proteins and DNAs,[11−15] viral nanoparticles (*e.g.*, virosomes and virus-like particles),[16−20] bacterially derived minicells and bacterial ghosts,[9,10,21] and mammalian cell-derived microparticles and exosomes.[22−24] All such biologically derived nanocarriers are intrinsically biodegradable and are capable of carrying a diverse payload for delivery at specific targeted sites.[9] Here, with the aim of developing biological vectors for targeted delivery of diverse therapeutic agents, we report the first application of engineered bacterial outer membrane vesicles (OMVs) as potential drug-delivery vehicles.

OMVs are nanosized (20−250 nm diameter), bilayered, spherical proteoliposomes that are continuously discharged from the surface of Gram-negative bacteria.[25−27] OMVs carry proteins screened by a sorting mechanism, resulting in selective localization of periplasmic and outer membrane proteins, including the 34 kDa pore-forming toxin ClyA.[26,28,29] Recent evidence indicates that genetic fusion between recombinant polypeptides and the C terminus of ClyA results in a functional display of recombinant protein on the surface of *Escherichia coli* and their derived OMVs.[28] Such C-terminal ClyA fusion partners are extended into the outside

* Address correspondence to (S. Jon) syjon@kaist.ac.kr.

Received for review November 4, 2013 and accepted January 10, 2014.

Published online January 10, 2014
10.1021/nn405724x

environment. In this process, the hemolytically active oligomeric conformation of ClyA is lost and no ClyA fusion-dependent cytotoxicity is observed.[28]

HER2 is a transmembrane receptor with tyrosine kinase activity that has an important role in cell growth regulation, survival, and differentiation.[30−32] Overexpression of HER2 is observed in 18−25% of breast cancers, ovarian cancers, gastric carcinoma, and salivary gland tumors and, therefore, presents an attractive target for both cancer diagnosis and therapy.[30,33,34]

In the current study, we sought to utilize the addressing property of ClyA to display a high-affinity, cancer-targeting ligand on the OMV surface and use such engineered OMVs for the purpose of targeted drug delivery. As a target, we selected HER2, using an anti-HER2 affibody for cancer-specific targeting because it has a very high affinity for HER2 (K_D = 22 pmol/L) and is small in size (58 amino acids).[34] OMVs with an anti-HER2 affibody ($Affi_{HER2}$OMVs) on the outer membrane surface were generated from ClyA-affibody-overexpressing *E. coli* and were loaded with therapeutic siRNA targeting kinesin spindle protein (KSP; also known as EG5). More importantly, we used a common laboratory *E. coli* K-12 W3110 strain carrying an msbB mutation, which is known to produce under-acylated lipopolysaccharide (LPS) and thus exhibits reduced endotoxicity toward human cells compared with *E. coli* strains that produce hexa-acylated LPS. Additionally, the shorter length of *o*-polysaccharide in LPS further reduces immunogenicity.[35−37]

RESULTS

Motivated by the goal of developing a strategy to utilize biological nanoparticles of bacterial origin as a drug-delivery vehicle, we designed and engineered bacterial OMVs displaying a HER2-specific affibody. In our approach, illustrated in Figure 1a and detailed below, bioengineered OMVs ($Affi_{HER2}$OMVs) were separated from impurities using extensive purification

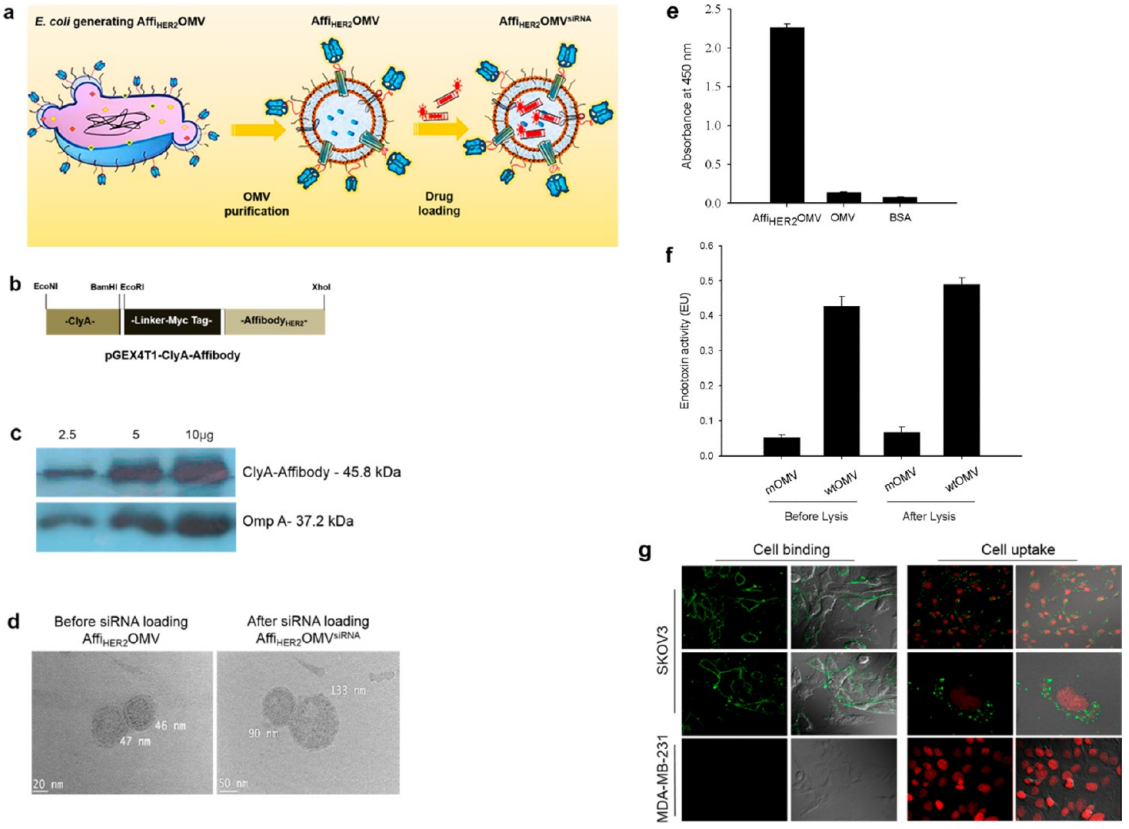

Figure 1. OMV purification and characterization. (a) Schematic representation of OMVs expressing HER2-specific affibody ($Affi_{HER2}$OMV), purified after vesiculation from the parent bacteria and further loaded with siRNA-TAMRA ($Affi_{HER2}OMV^{siRNA\text{-}TAMRA}$) using an electroporation method. (b) Schematic representation of the pGEX4T1-ClyA-Affibody construct. (c) Western blot analysis of ClyA-Affibody and native ompA in $Affi_{HER2}$OMV. Western blotting confirmed the localization of ClyA-Affibody in $Affi_{HER2}$OMV. (d) TEM micrograph revealing the nanosized (<200 nm), bilayered, circular morphology of $Affi_{HER2}$OMV (before siRNA loading) and $Affi_{HER2}OMV^{siRNA}$ (after siRNA loading). (e) ELISAs show the high specificity of $Affi_{HER2}$OMV for HER2 protein (~16-fold greater). The data are reported as the mean ± SD of three replicates. (f) Endotoxin activity was compared by LAL assay using 25 μg of OMVs; a difference of around 8-fold in activity was seen between modified OMVs (mOMVs) and wild-type OMVs (wtOMVs). No difference in activity was observed after the OMV lysis. (g) For cell-binding and uptake studies, HER2-overexpressing SKOV3 cells and HER2-negative MDA-MB-231 cells were co-incubated with $Affi_{HER2}$OMV (25 μg) and stained with an antiaffibody antibody (green), as described in Methods. Receptor-specific cell binding and uptake were seen only with HER2-overexpressing SKOV3 cells.

methods, and drug (siRNA) was loaded by electroporation. In addition, the fate of siRNA-loaded OMVs ($Affi_{HER2}OMV^{siRNA}$) was studied *in vitro* and *in vivo*.

OMV Isolation, Purification, and Characterization. Bacterial endotoxin-lipid A, an integral component of LPS, induces life-threatening inflammatory responses if injected systemically. A genetic mutation in the *E. coli* msbB gene results in loss of endotoxic activity by reducing the number of acyl chains in lipid A. Therefore, in the current study, $Affi_{HER2}$OMVs were produced from the msbB mutant *E. coli* K-12 W3110 strain transformed with a ClyA-affibody construct. To create the ClyA-Affibody construct, we genetically fused ClyA with an HER2-specific affibody containing an myc tag and connected *via* a flexible linker sequence (SSSSGSSSSG) (Figure 1b). $Affi_{HER2}$OMVs were purified by multiple centrifugation and filtration steps to ensure complete elimination of contaminants, such as parent bacterial debris and free endotoxins. The crude $Affi_{HER2}$OMVs obtained after preliminary purification were further separated using sequential density sucrose gradient ultracentrifugation (Supporting Information, Supplementary Figure 1a), followed by removal of free endotoxin using endotoxin-removing columns. Next, $Affi_{HER2}$OMVs were resuspended in 15% glycerol, passed through 0.20 μm cellulose acetate filters, and stored at −20 °C. Finally, to ensure that vesicles were free of bacteria, we plated $Affi_{HER2}$OMVs on growth agar plates and incubated plates at 37 °C overnight; the absence of bacterial colonies confirmed the sterility of $Affi_{HER2}$OMV preparations (data not shown). The expression of ClyA-Affibody recombinant protein in purified $Affi_{HER2}$OMVs was confirmed by Western blot analysis, which demonstrated the expression of ClyA-Affibody (45.8 kDa) along with that of the 37.2 kDa native outer membrane protein A (ompA) (Figure 1c). $Affi_{HER2}$OMVs were further characterized with respect to morphology and size using transmission electron microscopy (TEM) and electrophoretic light scattering (ELS) analysis techniques immediately before and after drug loading (Figure 1d; Supporting Information, Supplementary Figure 1b and c). These analyses revealed bilayered $Affi_{HER2}$OMVs of uniform circular morphology with diameters ranging from 30 to 250 nm. The specificity and exterior localization of anti-HER2 affibody were verified by enzyme-linked immunosorbent assays (ELISAs), which showed ~16-fold higher affinity of $Affi_{HER2}$OMVs for HER2 protein compared with control bovine serum albumin (BSA) protein or nontargeted OMVs, produced from plasmid-free msbB mutant *E. coli* (Figure 1e). Furthermore, using an LAL (Litmus Amebocyte Lysate) assay kit the endotoxin activity was measured with 25 μg of modified OMV and wild-type OMV (Figure 1f), produced respectively from msbB mutant *E. coli* K-12 W3110 strain transformed with a ClyA-affibody or wild-type *E. coli* K-12 W3110 strain. The endotoxin activity of modified OMV was about 8-fold lower than that of wild-type OMV; the endotoxin activities were unaffected even after the lysis of OMVs carried out to expose the lipid-A component of LPS, indicating the attenuation of endotoxicity due to the modifications of OMVs.

In order to confirm $Affi_{HER2}$-mediated cellular selectivity and receptor-mediated internalization, we monitored *in vitro* cell binding and uptake of $Affi_{HER2}$OMV by confocal imaging. For this purpose, we used mouse NIH3T3 fibroblast cells stably transfected with HER2 (referred to as NIH3T6.7), HER2-overexpressing SKOV3 cells, HER2-negative NIH3T3, and MDA-MB-231 cells. To determine HER2 specificity using a cell-binding approach, we incubated paraformaldehyde (PFA)-fixed, HER2-overexpressing and HER2-negative cells with $Affi_{HER2}$OMVs for 1 h at 4 °C and monitored the cell surface localization of $Affi_{HER2}$OMVs by confocal microscopy. The confocal images confirmed the specificity of $Affi_{HER2}$OMVs for HER2-overexpressing NIH3T6.7 and SKOV3 cells; surprisingly, no nonspecific binding was observed in control groups (Figure 1g; Supporting Information, Supplementary Figure 2, cell binding). To verify receptor-mediated uptake of $Affi_{HER2}$OMVs, we incubated HER2-overexpressing and HER2-negative cells with $Affi_{HER2}$OMVs for 2 h at 37 °C and, after washing, monitored the localization of $Affi_{HER2}$OMVs by confocal microscopy. Within 2 h of coincubation, a large proportion of HER2-overexpressing cells had incorporated $Affi_{HER2}$OMVs, whereas HER2-negative cells showed no uptake (Figure 1g; Supporting Information, Supplementary Figure 2, cell-uptake). Here, cellular localization of $Affi_{HER2}$OMVs was confirmed using an antiaffibody antibody. The green fluorescence signal of fluorescein isothiocyanate (FITC) revealed the binding and time-dependent uptake of $Affi_{HER2}$OMVs. Taken together, the findings of ELISAs and cell-binding and uptake studies show that the $Affi_{HER2}$OMVs selectively and effectively target HER2 and are rapidly internalized through receptor-mediated endocytosis.

siRNA Loading, Purification, and Quantification. In order to investigate the possibility of siRNA loading into $Affi_{HER2}$OMVs, we adapted an electroporation method using TAMRA-labeled siRNA against KSP (siRNA-TAMRA) as a model therapeutic agent. The TAMRA-labeled siRNA was further used in all *in vitro* analyses, whereas we used nonlabeled siRNA to investigate *in vivo* therapeutic efficacy. KSP is an ideal candidate for targeted cancer therapy because KSP mRNA is overexpressed in rapidly proliferating cells and tumor tissue compared to nonproliferating cells and normal adjacent tissues. KSP has an essential role in cell-cycle progression; KSP silencing blocks the formation of bipolar mitotic spindles, resulting in cell-cycle arrest and induction of apoptosis.[38−41] The electroporation method used here was developed empirically, as there is no currently established protocol for drug loading

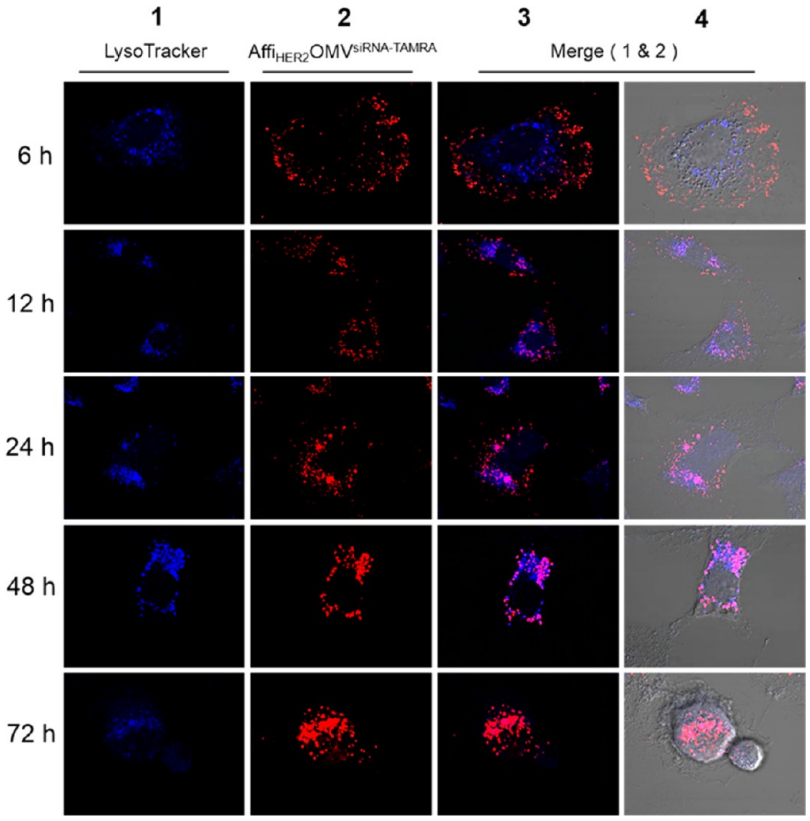

Figure 2. Intracellular trafficking of siRNA-loaded OMVs. SKOV3 cells showing the intracellular fate of siRNA-packaged (200 nM KSP siRNA) Affi$_{HER2}$OMV$^{siRNA-TAMRA}$ at different time points. SKOV3 cells were co-incubated with Affi$_{HER2}$OMV$^{siRNA-TAMRA}$ (red) for 2 h, and acidic compartments were stained with LysoTracker (blue); cells were monitored over the course of 72 h using a confocal microscope. Within 6 h of co-incubation, a large proportion of Affi$_{HER2}$OMV$^{siRNA-TAMRA}$ was internalized by the cells. At 12, 24, and 48 h, Affi$_{HER2}$OMV$^{siRNA-TAMRA}$ was concentrated in acidic compartments, which appeared pink due to co-localization. At 72 h, cytoplasmic siRNA was evident and most cells had adopted a circular morphology characteristic of dead cells, confirming siRNA escape and cytotoxic action.

into nanosized vesicles using electroporation. The red fluorescence of TAMRA, generated upon excitation at 550 nm, was helpful in monitoring siRNA loading and *in vitro* kinetics. The amount of siRNA loaded was assayed after removal of free siRNA by dialysis in phosphate-buffered saline (PBS) for 12 h. Electroporation at 700 V and 50 μF resulted in the high loading of siRNA in the OMV (~15 wt %; Supplementary Figure 3a and b) without producing changes in the membrane integrity of the OMV (Supplementary Figure 1b) as well as inducing the formation of siRNA aggregates (Supplementary Figure 3c). The same basic electroporation condition was followed for all subsequent experiments. TEM characterizations confirmed that siRNA loading did not alter morphology of Affi$_{HER2}$-OMVs, although a slight change in particle size was evident (Figure 1d; Supporting Information, Supplementary Figure 1b and c), demonstrating that the electroporation conditions were well tolerated.

Intracellular Trafficking of siRNA-Loaded Affi$_{HER2}$OMVs. The results of cell-specific binding and uptake studies encouraged us to investigate the intracellular kinetics of siRNA-loaded Affi$_{HER2}$OMVs. To accomplish this, we incubated SKOV3 cells with TAMRA-labeled KSP siRNA (red)-packaged OMVs (Affi$_{HER2}$OMV$^{siRNA-TAMRA}$) and monitored their fate for 72 h after uptake using confocal microscopy (Figure 2). We selected SKOV3 cells for kinetics studies because their large size and morphology make them well suited to single-cell imaging. Intracellular acidic compartments were stained using LysoTraker (navy blue). Within 6 h of co-incubation, large numbers of Affi$_{HER2}$OMV$^{siRNA-TAMRA}$ puncta (red) appeared within SKOV3 cells, corroborating our cell uptake analysis described above showing receptor-mediated endocytosis. Within 12 to 24 h of treatment, Affi$_{HER2}$OMV$^{siRNA-TAMRA}$ fluorescence was largely co-localized with markers of acidic compartments, which appeared pink. At 48 h, the fluorescence intensity attributable to coincident Affi$_{HER2}$OMV$^{siRNA-TAMRA}$ and LysoTracker staining reached a maximum; this indicates enhanced lysosomal acidification owing to uptake of a substantial amount of Affi$_{HER2}$OMV$^{siRNA-TAMRA}$, which would be predicted to enhance OMV degradation. SKOV3 cells appeared normal, exhibiting no major changes in cellular morphology. By 72 h, an increase in red fluorescence appeared in various parts of the cytosol, suggesting the escape of free siRNA from acidic compartments after the degradation of

Affi$_{HER2}$OMVs. At the same time, massive SKOV3 cell death was observed, as evidenced by adoption of a circularized morphology characteristic of dead cells (see additional 72 h images, Supporting Information, Supplementary Figure 4). These findings are consistent with inhibition of cell proliferation through siRNA-mediated degradation of KSP mRNA, suggesting that a therapeutically significant amount of free KSP siRNA managed to escape from the acidic compartments. To directly test this and validate the mechanism of cell death, we further evaluated KSP mRNA and protein level. The kinetics study described above confirmed the endocytosis of Affi$_{HER2}$OMV$^{siRNA\text{-}TAMRA}$ particles, reflecting their high specificity for HER2 and small size. Endocytosed Affi$_{HER2}$OMV^{siRNA} was found to follow the endosomal pathway, where the fate of Affi$_{HER2}$OMVs is to accumulate in the highly acidic lysosome compartment and slowly degrade. These findings corroborate those of Furuta *et al.*, who demonstrated complete degradation of OMVs inside lysosomes 48 h after endocytosis.[42,43] On the basis of these findings, we infer that OMVs have a very rigid and stable nanostructure. The slow release of siRNA under specific environmental conditions can mitigate the nonspecific toxicity caused by leakage of siRNA into the circulatory system. In addition, this slow-release property may provide sufficient time for siRNA to reach its target cancer cells in a region where the blood supply is abnormal. Although the specific mechanism of siRNA escape from acidic compartments is not known, a similar phenomenon was observed in earlier studies conducted using biological nanoparticles, such as bacterial minicells and exosomes.[21,23]

***In Vitro* Efficacy.** We quantitatively evaluated cell viability using the colorimetric, tetrazolium-based MTT assay. Three HER2-overexpressing cell lines (SKOV3, BT474, and HCC-1954) were treated for 96 h with PBS, Affi$_{HER2}$OMV$^{siRNA\text{-}TAMRA}$ (200 nM siRNA), OMV$^{siRNA\text{-}TAMRA}$ (nontargeted OMV carrying 200 nM siRNA), Affi$_{HER2}$OMV^{siNS} (Affi$_{HER2}$OMV carrying 200 nM nonspecific siRNA), and Free$^{siRNA\text{-}TAMRA}$ (200 nM siRNA). These analyses revealed that Affi$_{HER2}$OMV$^{siRNA\text{-}TAMRA}$ caused significant cytotoxicity in all three cell lines (Figure 3a), reducing viability in SKOV3, BT474, and HCC-1954 cells by ~73%, ~62%, and ~63%, respectively, compared to the respective PBS-treated control groups. Notably, Affi$_{HER2}$OMV^{siNS}, carrying a nonspecific (scrambled) siRNA, caused no cytotoxicity, indicating that the cell death observed in the Affi$_{HER2}$OMV$^{siRNA\text{-}TAMRA}$ treatment group may be due to KSP silencing (endocytosed Affi$_{HER2}$OMVs do not exert a cell-killing effect).

In order to establish the mechanism of cell death, we evaluated KSP silencing in the three different above-mentioned HER2-overexpressing cell lines after treatment with Affi$_{HER2}$OMV^{siRNA}. In agreement with the uptake of Affi$_{HER2}$OMV^{siRNA}, shown above,

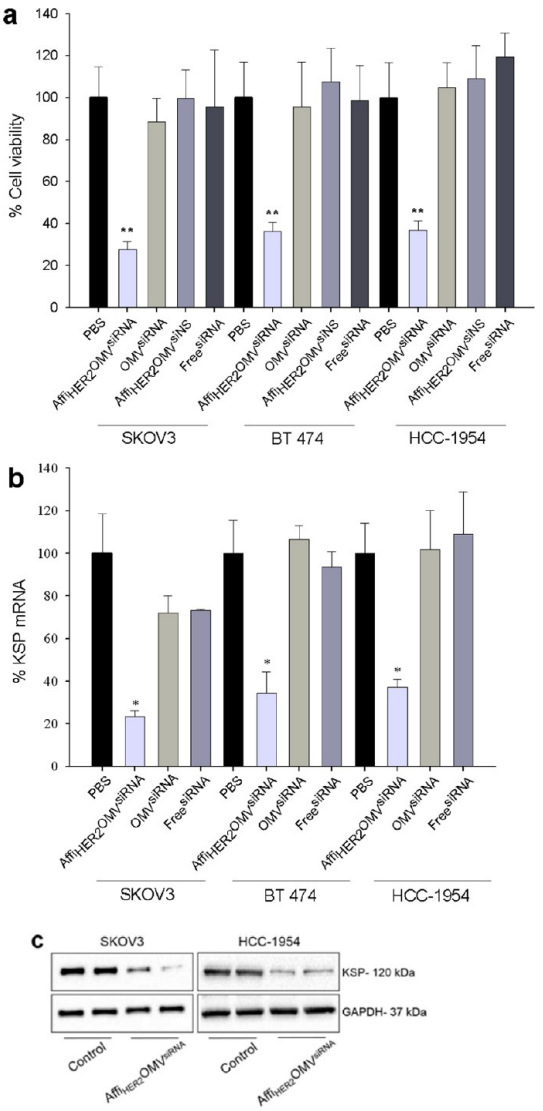

Figure 3. *In vitro* efficacy and gene silencing following siRNA delivery. Cell viability (by MTT assay) and KSP knockdown were monitored following delivery of Affi$_{HER2}$OMV^{siRNA} (200 nM siRNA) and compared with respective controls (each carries 200 nM siRNA except PBS control). (a) Cell viability was evaluated after 2 h of transfection and 96 h of incubation with Affi$_{HER2}$OMV^{siRNA} and controls. Affi$_{HER2}$OMV^{siRNA} treatment induced significant cytotoxicity compared with controls. Data represent means ± SD of five replicates, expressed relative to the PBS treatment group (indicates $p < 0.01$). (b) KSP mRNA levels were analyzed by qRT-PCR 72 h after transfection. KSP mRNA expression was significantly knocked down in Affi$_{HER2}$OMV^{siRNA}-treated groups compared to controls. SKOV3 cells were more sensitive to KSP siRNA than HCC-1954 and BT474 cells. Results are shown as mean ± SD of two replicates relative to the PBS treatment group. * indicates $p < 0.05$ *versus* PBS controls. (c) Western blot analyses were done for SKOV3 and HCC-1954 cells following transfection with Affi$_{HER2}$OMV^{siRNA}, as described above. Significant knockdown of KSP protein was evident in duplicate samples.**

quantitative (real-time) reverse transcription-polymerase chain reaction (qRT-PCR) analyses showed that KSP mRNA expression was significantly knocked down in SKOV3 (>70%), HCC-1954 (>60%), and BT747 (>60%) cells 72 h after treatment compared with unsilenced

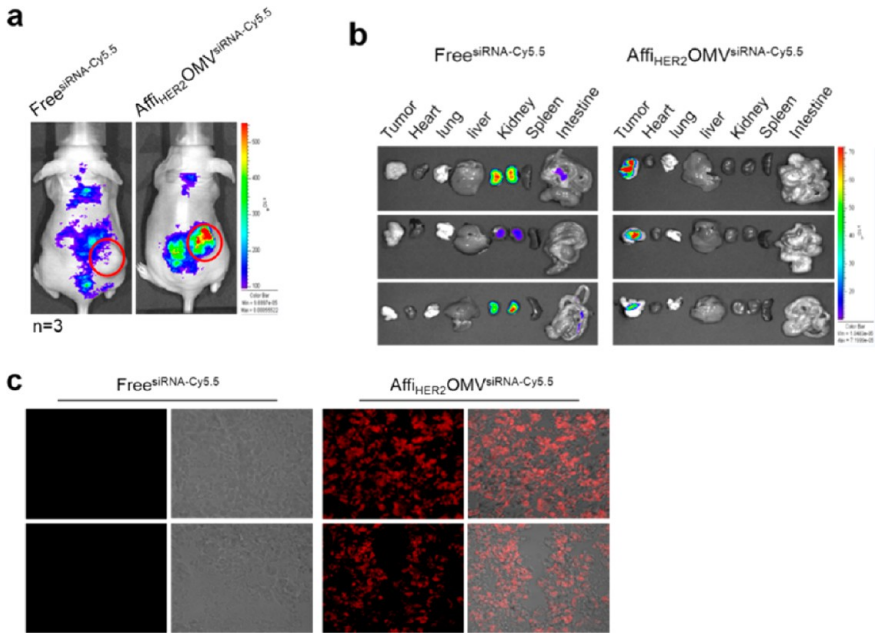

Figure 4. ***In vivo*** **tumor targeting and drug distribution. For optical imaging, HCC-1954 xenografts were given a single injection of 10 μg of Cy5.5-labeled free siRNA or an equivalent amount of Affi$_{HER2}$OMV$^{siRNA\text{-}Cy5.5}$** ***via*** **the tail vein (n = 3). Tissue-specific accumulation was confirmed 24 h postinjection using an IVIS-100 imaging system (Xenogen). (a) Whole-body** ***in vivo*** **imaging revealed high fluorescence due to accumulation of Affi$_{HER2}$OMV$^{siRNA\text{-}Cy5.5}$. The circles (red) indicate the tumor position. (b) Tumor tissues and major vital organs (heart, lung, liver, kidney, spleen, and intestine) were analyzed separately. IVIS images show tumor-specific retention and accumulation of delivered siRNA using the Affi$_{HER2}$OMV$^{siRNA\text{-}Cy5.5}$-based delivery system. (c) A confocal analysis of tumor sections shows the siRNA distribution in cancer cells treated with Affi$_{HER2}$OMV$^{siRNA\text{-}Cy5.5}$. No siRNA fluorescence was seen in animals treated with Free$^{siRNA\text{-}Cy5.5}$.**

levels of KSP mRNA in the PBS-treated control group (Figure 3b). Western blot analyses of SKOV3 and HCC-1954 cells showed that this decrease in KSP mRNA levels was accompanied by a substantial decrease in KSP protein expression (Figure 3b,c). The sensitivity of SKOV3 cells to KSP siRNA was greater than that of the other cell lines tested. For comparison purposes, we sought to test KSP silencing by transfecting cells with KSP siRNA using the commercially available reagent Lipofectamine. However, within 24 to 48 h of treatment, almost all cells had died (data not shown), possibly reflecting differences in siRNA loading efficiency and/or delivery mechanism; therefore, the gene silencing efficiency of our system could not be compared with available transfection reagents. We also examined mitotic arrest in response to KSP silencing by monitoring monoastral spindle formation by immunostaining for α-tubulin (green) and DNA (blue). Confocal images of spindle pole dynamics in SKOV3 cells treated with Affi$_{HER2}$OMV^{siRNA} exhibited a characteristic monoastral phenotype, indicating mitotic arrest due to KSP knockdown (Supporting Information, Supplementary Figure 5); in contrast, control cells showed either a normal bipolar spindle arrangement or cytoplasmic α-tubulin. These results indicate that the cytotoxic effects observed after siRNA delivery by Affi$_{HER2}$OMV^{siRNA} are solely due to KSP silencing.

In Vivo **Tumor Targeting and Antitumor Effect of HER2-Targeted, siRNA-Carrying OMVs.** To investigate *in vivo* tumor targeting and therapeutic efficacy, we systemically injected (*via* the tail vein) Affi$_{HER2}$OMV$^{siRNA\text{-}Cy5.5}$ carrying 10 μg of Cy5.5-labeled siRNA or free siRNA (10 μg) into HCC-1954 xenografts. The Affi$_{HER2}$OMV$^{siRNA\text{-}Cy5.5}$-administered xenografts showed high fluorescence in tumors even 24 h after treatment, a time when most Free$^{siRNA\text{-}Cy5.5}$ had been cleared, indicating tumor-selective accumulation of HER2-targeted Affi$_{HER2}$OMV$^{siRNA\text{-}Cy5.5}$ (Figure 4a). Furthermore, tissue imaging of all three animals in respective groups was carried out. Analysis shows that after 24 h of treatment, Affi$_{HER2}$OMV$^{siRNA\text{-}Cy5.5}$ was largely localized in tumor tissues compared to other vital organs (Figure 4b). We extended this analysis by assessing Affi$_{HER2}$OMV$^{siRNA\text{-}Cy5.5}$ distribution in tumor sections using confocal microscopy. Cy5.5-labeled siRNA fluorescence was detected in the majority of cells in tumor sections of Affi$_{HER2}$OMV$^{siRNA\text{-}Cy5.5}$-treated animals, whereas no fluorescence was detected in tumor sections of mice injected with Free$^{siRNA\text{-}Cy5.5}$ (Figure 4c). Taken together, these findings suggest that Affi$_{HER2}$OMV$^{siRNA\text{-}Cy5.5}$ has very high specificity for HER2-overexpressing tumor tissues. Importantly, the vesicles remained at the targeted site for several hours, ensuring the effective delivery of the cargo.

We next evaluated the antitumor effects of Affi$_{HER2}$OMV^{siRNA} in HCC-1954 xenografts. Eight to ten days after the inoculation of HCC-1954 cells, mice were divided into four groups (n = 5 mice/group): (1) vehicle

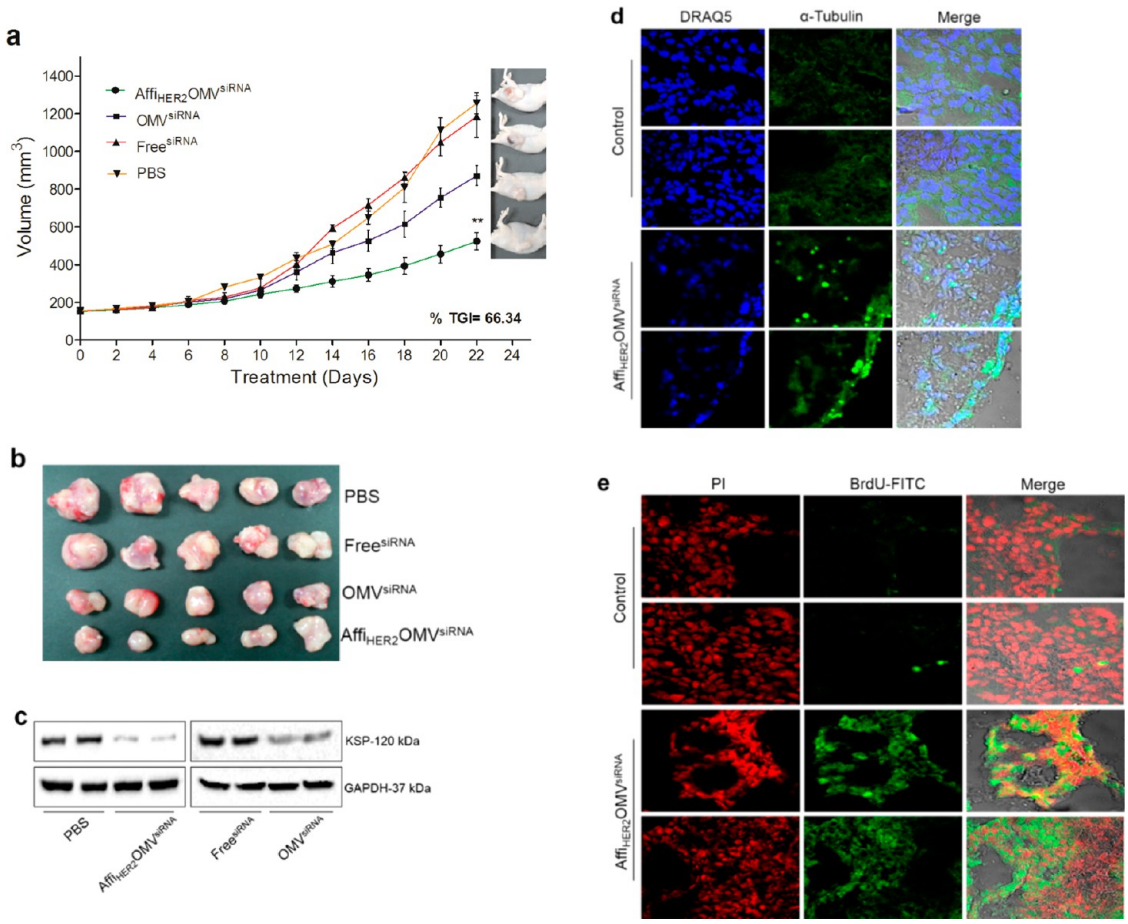

Figure 5. ***In vivo*** **antitumor effect of HER2-targeted, siRNA-carrying OMVs. (a) Tumor growth inhibition (TGI) was monitored in HCC-1954 xenografts. Mice were treated intravenously (siRNA per dose, ~4 μg) on alternate days to day 22. Affi$_{HER2}$OMV^{siRNA} exerted potent antitumor effects compared to all controls (**$p < 0.01$); each value represents the mean ± SD ($n = 5$ mice/group). (b) Dissected tumor tissues obtained from each group are shown, demonstrating differences in size. (c) Immunoblots of total protein show substantial KSP silencing in Affi$_{HER2}$OMV^{siRNA}-treated mice, analyzed in duplicate. (d) Immunofluorescence images showing the condensed α-tubulin structure in dead cells of tumor tissue. (e) TUNEL assays were carried out to visualize apoptotic cells in tumor sections. BrdU-FITC staining (green) confirmed the presence of large numbers of apoptotic cells in the tumor tissues of animals treated with Affi$_{HER2}$OMV^{siRNA} compared with PBS controls.**

control (DPBS-treated), (2) Free^{siRNA}, (3) nontargeted OMV^{siRNA}, and (4) HER2-targeted Affi$_{HER2}$OMV^{siRNA}. Mice were treated intravenously (siRNA per dose, ~4 μg) every other day for a total of 12 injections. The drug treatment started when tumor volume had reached ~150 mm^3. Tumor volumes and body weights were monitored throughout treatment, and tumor growth inhibition (TGI) was determined on the final day. In mice injected with Affi$_{HER2}$OMV^{siRNA}, tumor growth was delayed significantly compared to those injected with nontargeted OMV^{siRNA}, DPBS, or Free^{siRNA} (Figure 5a). The % tumor growth inhibition (%TGI) in the Affi$_{HER2}$OMV^{siRNA}-treated group compared to vehicle control was 66.34%. Next, tumors were harvested from animals in each group (Figure 5b) and analyzed for size and mechanism of cell killing (Figure 5c–e). Consistent with the observed delay in tumor growth, the volumes of excised tumors in the HER2-targeted Affi$_{HER2}$OMV^{siRNA} group were smaller than those in other treatment groups (Figure 5b). Importantly, Western blot analyses of excised tumors showed that the enhanced antitumor efficacy of HER2-targeted Affi$_{HER2}$OMV^{siRNA} was associated with a substantial reduction in KSP protein levels (Figure 5c). In keeping with this, we observed an α-tubulin staining pattern characteristic of the monoastral phenotype in the cells of tumor tissue from the HER2-targeted Affi$_{HER2}$OMV^{siRNA} group (Figure 5d); this pattern is similar to that detected in cultured cells upon KSP silencing, confirming the mechanism of the therapeutic effect. Moreover, TUNEL (terminal deoxynucleotidyl transferase dUTP nick-end labeling) assays detected abundant apoptotic cells in respective tumor sections (Figure 5e). Collectively, these results indicate that Affi$_{HER2}$OMV^{siRNA} exerts antitumor effects by selectively targeting and delivering siRNA to HER2-overexpressing tumors; the subsequent inhibition of KSP expression causes mitotic arrest, which results in apoptosis in targeted tumor tissue.

Investigation of Immune and Cytotoxic Responses. Safety issues are obviously an important concern in cases

where a bacterially derived product is given systemically. OMVs carry several bacterial proteins, virulence factors including surface factors that can mediate adhesion to host cells.[27] In addition a large portion of their outer membrane is covered with LPS, which could activate Toll-like receptors (TLRs) to elicit potent inflammatory responses.[27] We thus investigated OMV-induced immune responses both *in vitro* and *in vivo* by evaluating cytokine profiles and monitoring cytotoxicity and mortality. In our *in vitro* studies, we stimulated human monocyte THP1 cells for 24 h with OMVs generated from either msbB mutant *E. coli* carrying affibody plasmid (mOMV) or a wild-type strain (wtOMV). Both LPS (positive control) and wtOMV treatment induced a significantly greater increase in tumor necrosis factor (TNF)-α levels compared to mOMV treatment (Supporting Information, Supplementary Figure 6a). These findings are in accord with a study that reported that hexa-acylated LPS is more potent than penta-acylated LPS in stimulating the production of TNFα in THP1 cells.[35] Additionally, the surface modification of mOMVs with affibody might have prevented the internalization into THP1 cells to sufficient extent to trigger innate immune response, whereas with wtOMVs, which carry several membrane proteins and LPS, may enhance their adhesion and uptake to trigger immediate immune response. We also carried out *in vitro* cell toxicity and hemolysis studies to test the biocompatibility of OMVs. For the cell toxicity study, human umbilical vein endothelial cells (HUVECs) were treated with mOMVs or wtOMV for 4 h and after washing further incubated for 24 h. The treated cells appeared normal, as no signs of apoptosis was evident. The cell viability assay (MTT) further supported that no significant cytotoxicity was evident in mOMV-treated cells compared to wtOMV-treated cells (Supplementary Figure 6b, and c). To verify that the ClyA-affibody fusion protein is hemolytically inert, we plated $Affi_{HER2}$OMVs on blood agar plates under standard incubation conditions. $Affi_{HER2}$OMVs did not induce hemolysis, indicating that ClyA fusion proteins are in an inactive state (Supporting Information, Supplementary Figure 6d). This *in vitro* safety study profile indicated that engineered OMVs are safe for further *in vivo* analysis. Thus, we next investigated whether systemic injection of mOMVs in mice overstimulates the immune system and results in systemic disorders or death. Immune responses were recorded in C57BL/6 mice after repeated intravenous (iv) administration of either mOMVs or wtOMVs (10 and 20 μg) for 4 d. Within the first few hours of the final treatment (between 1 and 3 h), a comparison of wtOMV and mOMV treatment groups showed a slight increase in serum TNFα, IL-6, and IFNγ levels, which returned to nearly basal levels at 24 h (Figure 6). Neither treatment resulted in lethality, although body weight loss and hypothermia were more prominent in animals treated with wtOMVs (data not shown). Moreover, wtOMVs were more active in stimulating serum cytokine production than mOMVs. The initial rise in cytokine levels upon treatment with either form of OMV may have been due to the ability of enriched outer membrane proteins and LPS to induce the systemic release of cytokines. However, the differences in immunostimulation and the normalization of cytokine levels within 24 h indicate that mOMVs are well tolerated and do not induce severe host immune responses or prolonged inflammatory cytokine responses. Finally, we further investigated lethality by injecting a single dose of either form of OMV (up to 100 μg). The mOMVs caused no mortality at any dose, whereas wtOMVs at doses of 50 μg or higher caused mortality in all mice within 48 h of injection (data not shown). Collectively, these findings indicate clear differences in the endotoxic and immunogenic potentials of OMVs carrying wild-type *versus* under-acylated LPS. As such, these modified OMVs could be utilized safely to deliver therapeutic cargos *in vivo*.

DISCUSSION

Bacteria or their derived products are considered pathogenic, a primary safety concern that limits their clinical application.[9] Attenuated bacterial strains with no substantial pathogenicity or toxicity can be employed in the development of cargos for vaccines or therapeutic agents.[9] Hexa-acylated lipid A, an integral, proinflammatory component of LPS that stimulates the immune system by activating TLR pathways, shows a several-fold reduction in systemic toxicity if modified through under-acylation.[35−37] Mutational inactivation of the msbB gene in *E. coli* yields an engineered strain that produces such under-acylated (penta-acylated) lipid A-containing LPS and exhibits substantially reduced TLR-dependent stimulation of the host immune system.[36,37] In the current study, we developed bacterial OMVs with the penta-acylated LPS form, the engineered bacterial strain that possessed low endotoxicity. Such modifications in LPS resulted in reduced virulence compared to the wild type. Importantly, because of their short under-acylated LPS and surface modification with a cancer-targeting ligand, bioengineered OMVs evoked weak immunogenic responses and were well tolerated even after repeated iv administration. The short-lived cytokine responses revealed by analyzing early and delayed serum cytokine levels indicate that the modified OMVs do not elicit their antitumor effects by overstimulating inflammatory or immunological pathways. In addition, $Affi_{HER2}$OMVs caused no mortality, even after multiple systemic injections. The alteration in LPS and surface modification with affibody may result in reduced pathogenicity of OMVs by preventing their nonspecific interaction or entry into nontargeted host cells. However, it does not overrule the necessity for a detailed analysis of mOMV−host cell interactions

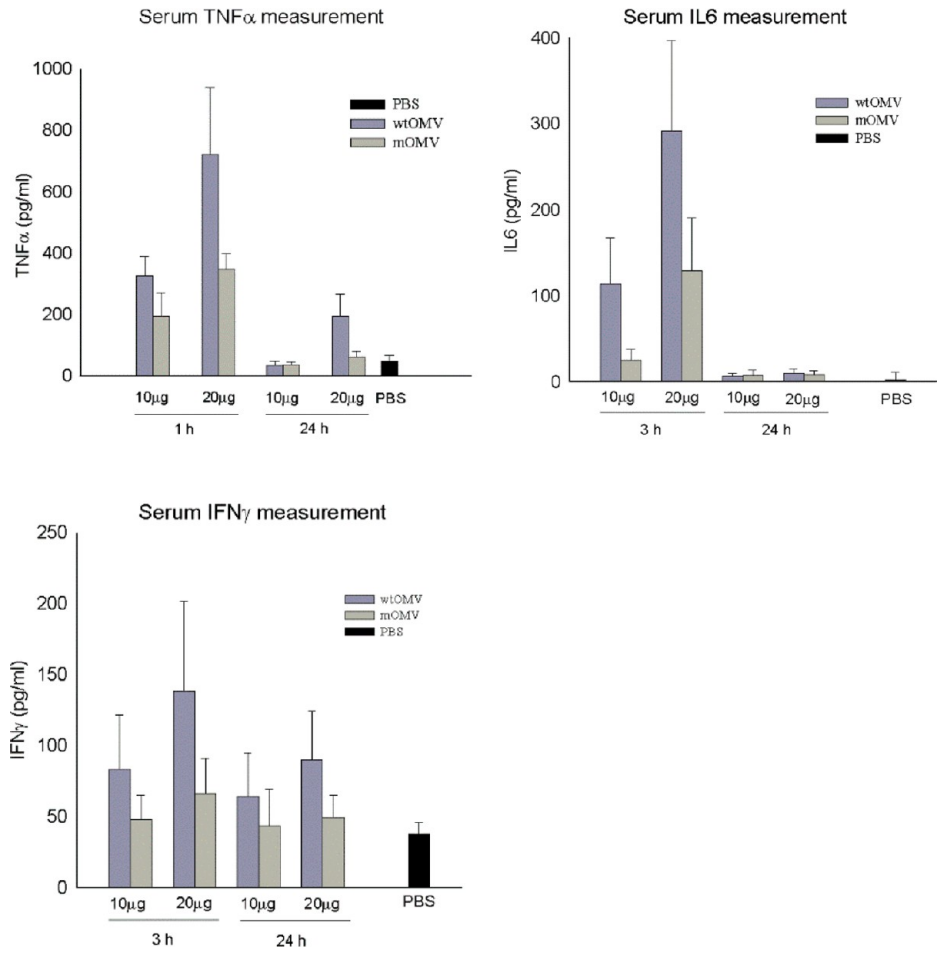

Figure 6. Investigation of immune responses in mice. Serum levels of TNFα, IL6, and IFNγ in C57BL/6 mice were quantified at two time points (1−3 and 24 h) after systemic administration of PBS, wtOMVs, or mOMVs (10 and 20 μg) for four consecutive days. Treatment with wtOMVs markedly enhanced serum levels of TNFα, IL6, and IFNγ within 3 h of treatment compared to mOMV treatment. However, cytokine levels in all groups returned to nearly basal levels by 24 h. Each value represents the mean ± SD (*n* = 5 mice/group) of two replicates, analyzed as described in Methods.

and antibody responses in higher animals (mammals) to draw conclusions about safety and toxicity.

We demonstrated the possibility of loading siRNA into the engineered OMVs. For this, we employed a simple electroporation method that was well tolerated, as evident from the intact circular morphology and integrity of OMVs after siRNA loading. Although OMVs could encapsulate only ~15% of KSP-siRNA, the amount was sufficient to exert cytotoxic effects when delivered in a cell-specific manner using HER2-homing $Affi_{HER2}$OMVs. The anticancer activity of $Affi_{HER2}$-OMV^{siRNA} was demonstrated using three different HER2-overexpressing cell lines, and in each case, targeted siRNA delivery resulted in significant inhibition of cell proliferation. The substantial knockdown of KSP mRNA and protein together with generation of the characteristic monoastral spindle arrangement in $Affi_{HER2}OMV^{siRNA}$-treated cells specifically link RNAi-mediated target knockdown and cancer cell death.

Our *in vivo* studies also show that $Affi_{HER2}OMV^{siRNA}$ accumulates selectively in the tumor tissue when administered systemically, as evidenced by the substantial amount of fluorescently labeled siRNA in most cancer cells. These findings indicate a rapid uptake of $Affi_{HER2}OMV^{siRNA}$ from tumor tissue due to extravasation. Importantly, the $Affi_{HER2}OMV^{siRNA}$ are small (<200 nm diameter), stable, and rigid. Therefore, they were able to target cancer tissues by the EPR effect and were not susceptible to the drug leakage or degradation in the circulation that occurs commonly with polymeric or liposome-based carriers.[9] The $Affi_{HER2}OMV^{siRNA}$, when administered repeatedly through the tail vein, significantly inhibited tumor growth. The very small amount of siRNA delivered using targeted OMVs was sufficient to exert a much more substantial inhibition of tumor growth inhibition than that produced by nontargeted delivery systems or free siRNA. However, a partial tumor growth regression was also observed from the nontargeted OMV^{siRNA}-treated group. These *in vivo* findings may show discrepancy from our *in vitro* analysis, where no nonspecific binding, uptake, or cytotoxicity was evident. This may be due to the very high specificity of $Affi_{HER2}OMV^{siRNA}$ that was endocytosed immediately

after the co-incubation and the unbound OMV^{siRNA} were cleared by manual washing. Whereas in the *in vivo* experiments, OMVs due to their small size accumulate in the tumor tissue by EPR effect and remain in the tumor interstitium for relatively longer duration. Therefore due to the incomplete clearance, the nonspecific uptake (by passive targeting) and siRNA delivery are possible in the OMV^{siRNA}-treated group, which may lead to the partial tumor regression by KSP silencing. Although the nontargeted OMV^{siRNA} group showed partial tumor regression, it turned out that the active HER2 targeting of OMVs could offer a clear advantage over passively targeted OMVs.

CONCLUSION

In conclusion, we report the first example of active tumor targeting using bacterially derived OMVs that are bioengineered to reduce their endotoxicity and express a cancer-specific targeting ligand to deliver their payload in a cell-selective manner. The great upsides of an engineered OMV-based delivery system is the possibility to re-engineer and target cancers specifically, low endotoxic potential, ability to package siRNA, ability to administer repeatedly through a systemic route, and ability to produce on a large scale *via* cost-effective bacterial fermentation. The developed system accumulates specifically in the tumor tissue and releases the drug, which resulted in cytotoxic effects and retardation of tumor growth. Due to their specificity, it offers the benefits of reduced side effects, a major factor limiting cancer therapy. We anticipate that studies of bacterial nanovesicles will be a valuable contribution to the development of novel biological particles for cancer therapy. In the future, we plan to investigate the possibility of loading diverse chemotherapeutic agents and test their fate *in vivo*.

METHODS

Bacterial Strains and Plasmid Construction. The msbB mutant W3110, a K12-derived *E. coli* strain, was kindly provided by Prof. Sang Hyun Kim (KRIBB, Republic of Korea). The ClyA gene was amplified from the W3110 *E. coli* genome and cloned into the pGEX4T1 vector (GE Healthcare). The vector was modified slightly to replace the GST tag with the ClyA gene at *Eco*NI and *Bam*HI restriction sites. Next, the affibody with an N-terminal myc tag and linker sequence (SSSSGSSSSG) was placed downstream of ClyA at *Eco*RI and *Xho*I restriction sites, yielding a C-terminal fusion of ClyA to the affibody with a myc tag and an intervening flexible linker. The pGEX4T1-ClyA-Affibody construct was transformed into the msbB mutant W3110 and utilized for generation of engineered OMVs. The expression of ClyA-Affibody in Affi$_{HER2}$OMVs was confirmed by immunoblotting.

Cell Culture. NIH3T3 mouse fibroblast cells stably transfected with HER2, referred to as NIH3T6.7 (kindly provided by Prof. Yong-Min Huh, Department of Radiology & Department of Biochemistry and Molecular Biology, Yonsei University, Seoul), cells were cultured in Dulbecco's modified Eagle medium (DMEM) supplemented with 10% fetal bovine serum (FBS; Gibco) and antibiotics. SKOV3 cells and HCC-1954 cells were cultured in RPMI-1640 medium containing 10% FBS and antibiotics. BT474 cells were cultured in Hybri-Care medium (ATCC) containing 10% FBS and antibiotics. HUVECs were cultured in F-12K medium containing endothelial cell growth supplements. All cells were incubated at 37 °C in 5% CO_2. Cell lines were purchased from Korean Cell Line Bank (KCLB; Seoul, Korea).

Dye-Labeled siRNAs. siRNAs labeled with TAMRA or Cy5.5 were purchased from ST Pharm Co. Ltd., Republic of Korea. The following siRNAs with the indicated sequences were used for this study: KSP-specific siRNA, 5′-CUG AAG ACC UGA AGA CAA UdTdT-3′ (sense) and 5′-AUU GUC UUC AGG UCU UCA GdTdT-3′ (antisense); and siNonsense (siNS), 5′-UGU AGA UGG ACU UGA ACU UdTdT-3′ (sense) and 5′-GAG UUC AAG UCC AUC UAC AdTdT-3′ (antisense).

OMV Generation, Purification, and Characterization. Affi$_{HER2}$OMVs were produced from the msbB mutant W3110 strain transformed with pGEX4T1-ClyA-affibody construct according to a previously described protocol, with slight modifications.[36] Briefly, *E. coli* were inoculated into 1000 mL of LB broth. After the culture had reached an optical density at 600 nm (OD_{600}) of 0.5−0.6, protein expression was induced by addition of 1 M isopropyl β-D-1-thiogalactopyranoside (IPTG; diluted 1:1000 in bacterial culture), and the culture was incubated overnight at 20 °C. The bacterial cells were removed by centrifugation at 5000*g* for 30 min at 4 °C. The resulting supernatant was filtered by passing through 0.45 μm filters (Nalgene, Thermo Scientific) and concentrated to 100 mL using 100 K Ultrafiltration Membranes (Millipore). The concentrate was precipitated using ammonium sulfate (final concentration, 400 g/L) at 4 °C overnight. The crude Affi$_{HER2}$OMVs obtained after centrifugation at 11000*g* for 30 min were washed twice with PBS by centrifugation at 45 000 rpm at 4 °C for 2 h (Beckman Coulter Optima TLX-120 ultracentrifuge). For purification, the resulting pellet was resuspended in PBS, layered over a sucrose gradient (1 mL each of 2.5, 1.6, 0.6 M sucrose), and separated by ultracentrifugation at 44 000 rpm for 20 h at 4 °C (Beckman Optima L-100 k ultracentrifuge; sw60Ti rotor). The Affi$_{HER2}$OMV fraction was collected carefully and washed twice with PBS by ultracentrifugation at 45 000 rpm at 4 °C for 1 h. The pellet was finally resuspended in 1 mL of 15% glycerol, passed through Detoxi-Gel endotoxin-removing columns (Thermo Scientific) to remove free endotoxin, filtered using 0.20 μm cellulose acetate filters (DISMIC-25cs), and stored at −20 °C until use. The sterility of Affi$_{HER2}$OMV preparations was confirmed by the absence of bacterial colonies in growth agar plates plated with Affi$_{HER2}$OMVs and grown overnight at 37 °C. The total protein concentration of Affi$_{HER2}$OMVs was quantified using a bicinchoninic acid assay (BCA protein assay kit; Thermo Scientific) according to the manufacturer's instructions. Affi$_{HER2}$OMVs were characterized with respect to size and morphology using an ELS 8000 electrophoretic light-scattering apparatus (Otsuka Electronic) and TECNAI F20 electron microscope (Phillips Electronic Instruments Corp.), respectively. For TEM analysis, Affi$_{HER2}$OMV samples were dropped onto a copper grid (200 mesh) and allowed to dry for 8−10 h. The samples were stained with 2% uranyl acetate for 10 min and washed by dipping into distilled water five times. Finally, grids were dried overnight in a desiccator. The dried copper grids were examined under a transmission electron microscope.

Monitoring OMV Specificity for HER2 by ELISA. The specificity of Affi$_{HER2}$OMVs for HER2 protein was determined by ELISA, according to a previously described protocol,[44] with slight changes. Briefly, the HER2 protein was coated onto 96-well plates (Corning) by adding 100 μL of HER2 protein and BSA protein (10 μg/mL in PBS) to each well and incubating plates at 4 °C overnight. After removal of the coating solution, 200 μL of blocking buffer (PBS containing 2% skim milk) was added to each well, and plates were incubated for 2 h at 25 °C. The blocking buffer was removed, and each well was washed six times with PBS containing 0.1% Tween-20 (PBST). Affi$_{HER2}$OMVs or nontargeted OMVs (100 μL) were added into each well and incubated for 2 h at 25 °C. Plates were washed as previously described, and Affi$_{HER2}$OMVs were detected by adding 100 μL of

a goat polyclonal antiaffibody antibody (Abcam) in PBST containing 2% skim milk. Plates were washed as above and incubated with horseradish peroxidase (HRP)-conjugated secondary antibody. Immunoreactivity was visualized by incubating with the chromogenic HRP substrate 3,3′,5,5′-tetramethybenzidine (TMB; BD OptEIA) and measuring absorbance at 450 nm.

Evaluation of the Endotoxin Activity. The endotoxicity of OMVs was evaluated using the LAL chromogenic endotoxin quantification kit (Thermo scientific) as per the manufacturer's instructions. We tested the activity of 25 μg of modified OMV and wild-type OMV in the intact form and after lysis carried out using 0.5% sodium deoxycholate.

Intracellular Trafficking of siRNA-Loaded OMVs. Intracellular trafficking studies were performed as described previously, with slight changes in the protocol.[21] Briefly, SKOV3 cells in RPMI-1640 medium containing 10% FBS and antibiotics were cultured on gelatin-coated coverslips in 12-well dishes. After cells had reached 70% confluence, the medium was replaced with OPTIMEM medium (Gibco) and cells were incubated for 30 min. $Affi_{HER2}OMV^{siRNA}$ ($Affi_{HER2}$OMVs loaded with 200 nM KSP siRNA) was then added, and cells were incubated for 2 h. The cells were then washed twice with PBS, and fresh RPMI-1640 medium containing 10% FBS and antibiotics was added. The acidic compartments of cells were stained with LysoTracker Blue DND-22 (Invitrogen) immediately before fixing, as per the manufacturer's instructions. At specific co-incubation time points (6, 12, 24, 48, and 72 h), cells on glass slides were washed with PBS and fixed with 4% (w/v) PFA, and coverslip were mounted using fluorescence mounting medium (Dako). All samples were examined using a confocal microscope equipped with 40× and 60× oil-immersion lenses.

RNA Preparation and Quantitative Real-Time PCR. Total RNA from cultured cells was isolated 72 h after incubating with $Affi_{HER2}OMV^{siRNA}$ ($Affi_{HER2}$OMVs loaded with 200 nM KSP siRNA) using an RNA purification kit (Hybrid-RTM, Gene All) according to the manufacturer's protocol. RNA samples were stored at −80 °C until use. RNA was reverse-transcribed using the ImProm-II Reverse Transcription System (Promega) according to the manufacturer's instructions. Quantitative real-time PCR was performed in 20 μL reactions using SYBR Premix (Kapa Systems) and a Rotor gene Q System (Qiagen). mRNA transcripts were quantified using the comparative Ct method, and the expression levels for target transcripts were presented as the ratio of the targets, normalized to the endogenous reference (GAPDH). Amplifications were performed using the following primer pairs: KSP, 5′-GGC GTC GCA GCC AAA TTC GTC-3′ (forward) and 5′-TGC CAG TTT GGC CAT ACG CA-3′ (reverse); GAPDH, 5′-CGT CTT CAC CAC CAT GGA GA-3′ (forward) and 5′-CGG CCA TCA CGC CAC AGT TT-3′ (reverse).

Protein Immunoblotting. Protein expression was assessed by Western blotting. For *in vitro* studies, SKOV3 and HCC-1954 cells were lysed 72 h after incubation with $Affi_{HER2}OMV^{siRNA}$ ($Affi_{HER2}$OMVs loaded with 200 nM KSP siRNA); for *in vivo* studies, tumor tissues were harvested immediately after the last treatment. For all samples, total protein concentration was determined by Bradford assay, and an equal amount of total protein in lysates (30 μg) was separated by sodium dodecyl sulfate-polyacrylamide gel electrophoresis (SDS-PAGE) on 12% gels followed by immobilization on a PVDF (polyvinylidene difluoride) membrane by electrotransfer. Blots were blocked by incubating with 5% nonfat dry milk for 1 h, probed with primary antibodies against KSP (mouse anti-EG5 monoclonal antibody; Abcam) and GAPDH (mouse monoclonal; Santa Cruz Biotechnology), and subsequently incubated with HRP-conjugated secondary antibodies. Immunoreactive proteins were visualized using Western blotting detection reagents (GE Healthcare) as per standard protocols.

Cell Viability Assay (MTT). MTT assays were performed as described previously with slight changes.[45] Briefly, SKOV3, HCC-1954, or BT474 cells were seeded into 96-well plates at 5×10^3 cells/well, incubated overnight, and then transfected with $Affi_{HER2}OMV^{siRNA}$, $Affi_{HER2}OMV^{siNS}$, or OMV^{siRNA} (loaded with 200 nM siRNA) for 2 h. The cells were washed and further incubated in fresh media. Approximately 96 h post-transfection, cells were washed twice with PBS, after which 100 μL of MTT solution (Enhanced Cell Viability Assay kit; DAEIL LAB Service Co., Ltd.) was added to each well and samples were incubated at 37 °C for 4 h. The resulting formazan product was dissolved by adding 200 μL of dimethyl sulfoxide (DMSO) to each well. The plates were read at 570 nm using a microplate reader.

Tumor Xenograft Model, *in Vivo* Targeting, and Antitumor Effects. Xenograft studies were performed using 6−8-week-old female Balb/c nude mice (Orient Bio Inc.) as described previously,[46] with slight changes. All animal experiments were performed according to established guidelines and with the approval of the Institutional Animal Care Committee (2012-BS07). Sample sizes for animal studies were chosen based on institutional recommendations with guidance from the literature. Investigators were not blinded to the identity of groups. HER2-overexpressing HCC-1954 cells (1×10^7) in 100 μL of 1:1 PBS/Matrigel (BD Biosciences) were implanted subcutaneously (sc) into the flanks of nude mice. Tumor volume, calculated as (length × width^2)/2, was monitored at regular intervals and was expressed as group mean ± standard deviation (SD). For optical imaging, mice were given a single injection of 10 μg of Cy5.5-labeled free siRNA or an equivalent amount of $Affi_{HER2}$-OMV^{siRNA} *via* the tail vein (n = 3). Tissue homing and retention were monitored at 24 h postinjection using an IVIS 100 imaging system (Xenogen). For the efficacy study, drug treatment started when tumor volume had reached ∼150 mm^3; mice were sacrificed after the last treatment. Ten to 12 days after implantation, mice were randomized into four groups based on body weight and tumor volume (n = 5 mice/group): (1) vehicle control (PBS), (2) free siRNA, (3) OMV^{siRNA}, and (4) $Affi_{HER2}$-OMV^{siRNA} (concentration of siRNA, ∼4 μg per dose). Mice were injected *via* the tail vein every other day for a total of 12 injections. Tumor volumes and body weights were monitored throughout treatment, and tumor growth inhibition was determined on the final day as TGI = 100% × ($T_{vol}^{Control} - T_{vol}^{Treated}$)/$T_{vol}^{Control}$, where T_{vol} = final tumor volume − initial tumor volume.[47] Differences with a p-value < 0.05 were considered significant. Tumor tissue was collected and analyzed for total KSP protein by immunoblotting. Monoastral phenotype was detected by immunostaining with an anti-α-tubulin antibody (Abcam), and apoptotic cells in tissue sections were visualized by TUNEL assay (Bio Vision) according to the manufacturer's instructions.

Serum Cytokine Analysis. Animal studies were performed using 6−8-week-old female C57BL/6 mice (Orient Bio Inc.) as per the guidelines of the Institutional Animal Care Committee. Mice were divided into three groups (n = 5 mice/group; one animal per group was kept as a substitution to replace any animal that died before completion of the study): (1) vehicle control (PBS), (2) wtOMV, and (3) mOMV (10 and 20 μg). Investigators were not blinded to the identity of groups. Agents were administered for four consecutive days through the tail vein. Blood was collected through the retro-orbital route at two time points (1−3 and 24 h) for monitoring of early and delayed responses. The serum cytokines, TNF-α, IL-6, and interferon (IFN)-γ were quantified using the respective ELISA kits (R&D Systems) by analyzing duplicate readings of each sample (at 450 nm), as per the manufacturer's instructions.

Statistics. Statistical analyses of data were performed using the SPSS 18.0 program by applying the nonparametric Kruskal−Wallis and Mann−Whitney U tests. Results are expressed as means ± SD, and differences are considered statistically significant for p-values < 0.05.

Conflict of Interest: The authors declare no competing financial interest.

Acknowledgment. This research was supported by the Bio & Medical Technology Development Program of the National Research Foundation (no. 2013035952) and by the Intelligent Synthetic Biology Center of Global Frontier Project funded by the Ministry of Science, ICT & Future Planning (no. 2013M3A6A8073557).

Supporting Information Available: OMV isolation and characterization (Supplementary Figure 1), cell-binding and uptake[48] studies (Supplementary Figure 2), siRNA loading and quantification

(Supplementary Figure 3), intracellular fate of siRNA-loaded OMVs after 72 h of treatment (Supplementary Figure 4), confirmation of KSP silencing by delivered siRNA *in vitro* (Supplementary Figure 5), and THP1 cell stimulation[49] and biocompatibility study (Supplementary Figure 6). This material is available free of charge *via* the Internet at http://pubs.acs.org.

REFERENCES AND NOTES

1. Petros, R. A.; DeSimone, J. M. Strategies in the Design of Nanoparticles for Therapeutic Applications. *Nat. Rev. Drug Discovery* **2010**, *9*, 615–627.
2. Soussan, E.; Cassel, S.; Blanzat, M.; Rico-Lattes, I. Drug Delivery by Soft Matter: Matrix and Vesicular Carriers. *Angew. Chem., Int. Ed.* **2009**, *48*, 274–288.
3. Farokhzad, O. C.; Langer, R. Impact of Nanotechnology on Drug Delivery. *ACS Nano* **2009**, *3*, 16–20.
4. Shi, J. J.; Votruba, A. R.; Farokhzad, O. C.; Langer, R. Nanotechnology in Drug Delivery and Tissue Engineering: From Discovery to Applications. *Nano Lett.* **2010**, *10*, 3223–3230.
5. Adair, J. H.; Parette, M. P.; Altinoglu, E. I.; Kester, M. Nanoparticulate Alternatives for Drug Delivery. *ACS Nano* **2010**, *4*, 4967–4970.
6. Peer, D.; Karp, J. M.; Hong, S.; Farokhzad, O. C.; Margalit, R.; Langer, R. Nanocarriers as an Emerging Platform for Cancer Therapy. *Nat. Nanotechnol.* **2007**, *2*, 751–760.
7. Hrkach, J.; Von Hoff, D.; Ali, M. M.; Andrianova, E.; Auer, J.; Campbell, T.; De Witt, D.; Figa, M.; Figueiredo, M.; Horhota, A.; *et al*. Preclinical Development and Clinical Translation of a Psma-Targeted Docetaxel Nanoparticle with a Differentiated Pharmacological Profile. *Sci. Transl. Med.* **2012**, *4*, 128 ra39.
8. Tan, S. J.; Kiatwuthinon, P.; Roh, Y. H.; Kahn, J. S.; Luo, D. Engineering Nanocarriers for siRNA Delivery. *Small* **2011**, *7*, 841–856.
9. Yoo, J. W.; Irvine, D. J.; Discher, D. E.; Mitragotri, S. Bio-Inspired, Bioengineered and Biomimetic Drug Delivery Carriers. *Nat. Rev. Drug Discovery* **2011**, *10*, 521–535.
10. MacDiarmid, J. A.; Mugridge, N. B.; Weiss, J. C.; Phillips, L.; Burn, A. L.; Paulin, R. P.; Haasdyk, J. E.; Dickson, K. A.; Brahmbhatt, V. N.; Pattison, S. T.; *et al*. Bacterially Derived 400 nm Particles for Encapsulation and Cancer Cell Targeting of Chemotherapeutics. *Cancer Cell* **2007**, *11*, 431–445.
11. MaHam, A.; Tang, Z. W.; Wu, H.; Wang, J.; Lin, Y. H. Protein-Based Nanomedicine Platforms for Drug Delivery. *Small* **2009**, *5*, 1706–1721.
12. Walsh, A. S.; Yin, H. F.; Erben, C. M.; Wood, M. J. A.; Turberfield, A. J. DNA Cage Delivery to Mammalian Cells. *ACS Nano* **2011**, *5*, 5427–5432.
13. Wang, K. L.; You, M. X.; Chen, Y.; Han, D.; Zhu, Z.; Huang, J.; Williams, K.; Yang, C. J.; Tan, W. H. Self-Assembly of a Bifunctional DNA Carrier for Drug Delivery. *Angew. Chem., Int. Ed.* **2011**, *50*, 6098–6101.
14. Lin, X.; Xie, J.; Niu, G.; Zhang, F.; Gao, H. K.; Yang, M.; Quan, Q. M.; Aronova, M. A.; Zhang, G. F.; Lee, S.; *et al*. Chimeric Ferritin Nanocages for Multiple Function Loading and Multimodal Imaging. *Nano Lett.* **2011**, *11*, 814–819.
15. Chang, M.; Yang, C. S.; Huang, D. M. Aptamer-Conjugated DNA Icosahedral Nanoparticles as a Carrier of Doxorubicin for Cancer Therapy. *ACS Nano* **2011**, *5*, 6156–6163.
16. Wu, W.; Hsiao, S. C.; Carrico, Z. M.; Francis, M. B. Genome-Free Viral Capsids as Multivalent Carriers for Taxol Delivery. *Angew. Chem. Int. Ed.* **2009**, *48*, 9493–9497.
17. Steinmetz, N. F.; Ablack, A. L.; Hickey, J. L.; Ablack, J.; Manocha, B.; Mymryk, J. S.; Luyt, L. G.; Lewis, J. D. Intravital Imaging of Human Prostate Cancer Using Viral Nanoparticles Targeted to Gastrin-Releasing Peptide Receptors. *Small* **2011**, *7*, 1664–1672.
18. Hooker, J. M.; Datta, A.; Botta, M.; Raymond, K. N.; Francis, M. B. Magnetic Resonance Contrast Agents from Viral Capsid Shells: A Comparison of Exterior and Interior Cargo Strategies. *Nano Lett.* **2007**, *7*, 2207–2210.
19. Tong, G. J.; Hsiao, S. C.; Carrico, Z. M.; Francis, M. B. Viral Capsid DNA Aptamer Conjugates as Multivalent Cell-Targeting Vehicles. *J. Am. Chem. Soc.* **2009**, *131*, 11174–11178.
20. Ashley, C. E.; Carnes, E. C.; Phillips, G. K.; Durfee, P. N.; Buley, M. D.; Lino, C. A.; Padilla, D. P.; Phillips, B.; Carter, M. B.; Willman, C. L.; *et al*. Cell-Specific Delivery of Diverse Cargos by Bacteriophage Ms2 Virus-like Particles. *ACS Nano* **2011**, *5*, 5729–5745.
21. MacDiarmid, J. A.; Amaro-Mugridge, N. B.; Madrid-Weiss, J.; Sedliarou, I.; Wetzel, S.; Kochar, K.; Brahmbhatt, V. N.; Phillips, L.; Pattison, S. T.; Petti, C.; *et al*. Sequential Treatment of Drug-Resistant Tumors with Targeted Minicells Containing siRNA or a Cytotoxic Drug. *Nat. Biotechnol.* **2009**, *27*, 643–U97.
22. Tang, K.; Zhang, Y.; Zhang, H. F.; Xu, P. W.; Liu, J.; Ma, J. W.; Lv, M.; Li, D. P.; Katirai, F.; Shen, G. X.; *et al*. Delivery of Chemotherapeutic Drugs in Tumour Cell-Derived Microparticles. *Nat. Commun.* **2012**, *3*, 1282.
23. Alvarez-Erviti, L.; Seow, Y. Q.; Yin, H. F.; Betts, C.; Lakhal, S.; Wood, M. J. A. Delivery of siRNA to the Mouse Brain by Systemic Injection of Targeted Exosomes. *Nat. Biotechnol.* **2011**, *29*, 341–U179.
24. Jang, S. C.; Kim, O. Y.; Yoon, C. M.; Choi, D. S.; Roh, T. Y.; Park, J.; Nilsson, J.; Lotvall, J.; Kim, Y. K.; Gho, Y. S. Bioinspired Exosome-Mimetic Nanovesicles for Targeted Delivery of Chemotherapeutics to Malignant Tumors. *ACS Nano* **2013**, *7*, 7698–7710.
25. Lee, E. Y.; Choi, D. S.; Kim, K. P.; Gho, Y. S. Proteomics in Gram-Negative Bacterial Outer Membrane Vesicles. *Mass Spectrom. Rev.* **2008**, *27*, 535–555.
26. Wai, S. N.; Lindmark, B.; Soderblom, T.; Takade, A.; Westermark, M.; Oscarsson, J.; Jass, J.; Richter-Dahlfors, A.; Mizunoe, Y.; Uhlin, B. E. Vesicle-Mediated Export and Assembly of Pore-Forming Oligomers of the Enterobacterial Clya Cytotoxin. *Cell* **2003**, *115*, 25–35.
27. Kuehn, M. J.; Kesty, N. C. Bacterial Outer Membrane Vesicles and the Host-Pathogen Interaction. *Gene Dev.* **2005**, *19*, 2645–2655.
28. Kim, J. Y.; Doody, A. M.; Chen, D. J.; Cremona, G. H.; Shuler, M. L.; Putnam, D.; DeLisa, M. P. Engineered Bacterial Outer Membrane Vesicles with Enhanced Functionality. *J. Mol. Biol.* **2008**, *380*, 51–66.
29. Chen, D. J.; Osterrieder, N.; Metzger, S. M.; Buckles, E.; Doody, A. M.; DeLisa, M. P.; Putnam, D. Delivery of Foreign Antigens by Engineered Outer Membrane Vesicle Vaccines. *Proc. Natl. Acad. Sci. U.S.A.* **2010**, *107*, 3099–3104.
30. Baselga, J.; Swain, S. M. Novel Anticancer Targets: Revisiting Erbb2 and Discovering Erbb3. *Nat. Rev. Cancer* **2009**, *9*, 463–475.
31. Hynes, N. E.; Lane, H. A. Erbb Receptors and Cancer: The Complexity of Targeted Inhibitors. *Nat. Rev. Cancer* **2005**, *5*, 341–354.
32. Yarden, Y.; Sliwkowski, M. X. Untangling the Erbb Signalling Network. *Nat. Rev. Mol. Cell Biol.* **2001**, *2*, 127–137.
33. Olayioye, M. A.; Neve, R. M.; Lane, H. A.; Hynes, N. E. The Erbb Signaling Network: Receptor Heterodimerization in Development and Cancer. *Embo J.* **2000**, *19*, 3159–3167.
34. Orlova, A.; Magnusson, M.; Eriksson, T. L. J.; Nilsson, M.; Larsson, B.; Hoiden-Guthenherg, I.; Widstrom, C.; Carlsson, J.; Tolmachev, V.; Stahl, S.; *et al*. Tumor Imaging Using a Picomolar Affinity Her2 Binding Affibody Molecule. *Cancer Res.* **2006**, *66*, 4339–4348.
35. Hajjar, A. M.; Ernst, R. K.; Tsai, J. H.; Wilson, C. B.; Miller, S. I. Human Toll-Like Receptor 4 Recognizes Host-Specific LPS Modifications. *Nat. Immunol.* **2002**, *3*, 354–359.
36. Kim, S. H.; Kim, K. S.; Lee, S. R.; Kim, E.; Kim, M. S.; Lee, E. Y.; Gho, Y. S.; Kim, J. W.; Bishop, R. E.; Chang, K. T. Structural Modifications of Outer Membrane Vesicles to Refine Them as Vaccine Delivery Vehicles. *Bba-Biomembranes* **2009**, *1788*, 2150–2159.
37. Somerville, J. E.; Cassiano, L.; Darveau, R. P. Escherichia Coli MsbB Gene as a Virulence Factor and a Therapeutic Target. *Infect. Immun.* **1999**, *67*, 6583–6590.
38. Jackson, J. R.; Patrick, D. R.; Dar, M. M.; Huang, P. S. Targeted Anti-Mitotic Therapies: Can We Improve on Tubulin Agents? *Nat. Rev. Cancer* **2007**, *7*, 107–117.

39. Judge, A. D.; Robbins, M.; Tavakoli, I.; Levi, J.; Hu, L.; Fronda, A.; Ambegia, E.; McClintock, K.; MacLachlan, I. Confirming the RNAi-Mediated Mechanism of Action of siRNA-Based Cancer Therapeutics in Mice. *J. Clin. Invest.* **2009**, *119*, 661–673.
40. Knight, S. D.; Parrish, C. A. Recent Progress in the Identification and Clinical Evaluation of Inhibitors of the Mitotic Kinesin KSP. *Curr. Top. Med. Chem.* **2008**, *8*, 888–904.
41. Tao, W. K.; South, V. J.; Zhang, Y.; Davide, J. P.; Farrell, L.; Kohl, N. E.; Sepp-Lorenzino, L.; Lobell, R. B. Induction of Apoptosis by an Inhibitor of the Mitotic Kinesin KSP Requires Both Activation of the Spindle Assembly Checkpoint and Mitotic Slippage. *Cancer Cell* **2005**, *8*, 49–59.
42. Amano, A.; Takeuchi, H.; Furuta, N. Outer Membrane Vesicles Function as Offensive Weapons in Host-Parasite Interactions. *Microbes Infect.* **2010**, *12*, 791–798.
43. Furuta, N.; Tsuda, K.; Omori, H.; Yoshimori, T.; Yoshimura, F.; Amano, A. Porphyromonas Gingivalis Outer Membrane Vesicles Enter Human Epithelial Cells *via* an Endocytic Pathway and Are Sorted to Lysosomal Compartments. *Infect. Immun.* **2009**, *77*, 4187–4196.
44. Kim, S.; Kim, D.; Jung, H. H.; Lee, I. H.; Kim, J. I.; Suh, J. Y.; Jon, S. Bio-Inspired Design and Potential Biomedical Applications of a Novel Class of High-Affinity Peptides. *Angew. Chem., Int. Ed.* **2012**, *51*, 1890–1894.
45. Bagalkot, V.; Farokhzad, O. C.; Langer, R.; Jon, S. An Aptamer-Doxorubicin Physical Conjugate as a Novel Targeted Drug-Delivery Platform. *Angew. Chem., Int. Ed.* **2006**, *45*, 8149–8152.
46. Yu, M. K.; Jeong, Y. Y.; Park, J.; Park, S.; Kim, J. W.; Min, J. J.; Kim, K.; Jon, S. Drug-Loaded Superparamagnetic Iron Oxide Nanoparticles for Combined Cancer Imaging and Therapy *in Vivo*. *Angew. Chem., Int. Ed.* **2008**, *47*, 5362–5365.
47. Letsch, M.; Schally, A. V.; Busto, R.; Bajo, A. M.; Varga, J. L. Growth Hormone-Releasing Hormone (Ghrh) Antagonists Inhibit the Proliferation of Androgen-Dependent and -Independent Prostate Cancers. *Proc. Natl. Acad. Sci. U.S.A.* **2003**, *100*, 1250–1255.
48. Yu, M. K.; Kim, D.; Lee, I. H.; So, J. S.; Jeong, Y. Y.; Jon, S. Image-Guided Prostate Cancer Therapy Using Aptamer-Functionalized Thermally Cross-Linked Superparamagnetic Iron Oxide Nanoparticles. *Small* **2011**, *7*, 2241–2249.
49. Takashiba, S.; Van Dyke, T. E.; Amar, S.; Murayama, Y.; Soskolne, A. W.; Shapira, L. Differentiation of Monocytes to Macrophages Primes Cells for Lipopolysaccharide Stimulation *via* Accumulation of Cytoplasmic Nuclear Factor Kappa B. *Infect. Immun.* **1999**, *67*, 5573–5578.